Open **S**ounce **C**ombustion **I**nstability **L**ow **O**rder **S**imulator (OSCILOS–Long)
Technical report for version 1.2

Jingxuan Li and Aimee S. Morgans
Department of Aeronautics, Imperial College London, UK
jingxuan.li@imperial.ac.uk and *a.morgans@imperial.ac.uk*

1 Introduction

Combustion instability has been a major issue in the design stage of the industrial gas turbine and aeroengine for decades. It arises due to the coupling between the unstable combustion process and acoustic disturbances within the combustion chamber. The mechanism can be briefly described as: acoustic noise with a broad frequency bandwidth is produced during the combustion process [1]. These sound waves propagate inside the combustion chamber, interact with the boundaries and return back to the combustion zone with a time delay that depends on the size of the combustion chamber, disturbances of speed of sound and impedances at the boundaries of the combustion chamber. These pressure oscillations generate in turn perturbations of the flow field by modifying the local flowrate, reactant composition or thermodynamic properties in the flame region, producing heat release rate disturbances [2, 3]. When these disturbances are synchronised, they amplify leading to an increase of acoustic energy in the system and a resonance is generally observed at specific tones. These self-sustained instabilities are more likely to happen in lean premixed combustion systems, which offer the potential for reducing NO_x emissions in modern gas turbine design [4].

Combustion instabilities are generally not desirable because they may lead to an early ageing of the combustion chamber or even to severe structural damage [5]. Knowledge of this complex mechanism is necessary in the development of control strategies. The open source combustion instability low-order simulator (OSCILOS) is an open source code for simulating combustion instability. It is written in Matlab® / Simulink® and is very straightforward to run and edit. It can simulate both longitudinal and annular combustor geometries. It represents a combustor as a network of connected modules. The acoustic waves are modeled as either 1-D plane waves (longitudinal combustors) or 2-D plane/circumferential waves (annular combustors). A variety of inlet and exit acoustic boundary conditions are possible, including open, closed, choked and user defined boundary conditions. The response of the flame to acoustic waves is captured via a flame model; flame models ranging from linear $n-\tau$ models to non-linear flame describing functions, either prescribed analytically or loaded from experiment / CFD data, can be prescribed. The mean flow is calculated simply by assuming 1-D flow conditions, with changes only across module interfaces or flames. This current version is for longitudinal modes. This assumes a longitudinal/cannular/can combustor geometry, or an annular geometry but where only plane acoustic waves are known to be of interest.

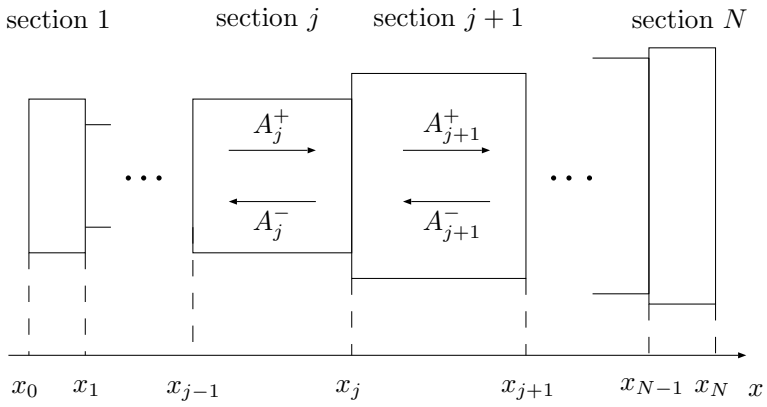

Figure 1: Schematic view of the long sectional area change combustor.

2 Acoustic wave equations

Analysis is carried out on a model combustion chamber which is schematically described in Figure 1. The configuration consists of several cylindrical tubes with different sectional areas. Denoting the distance along the longitudinal axis by the vector x, the inlet and outlet of section j are at $x = x_{j-1}$ and $x = x_j$ respectively, where $j = 1, 2, \ldots N$. A premixed gaseous flame located at $x = x_n$ (n is integer and $0 < n < N$) is used as the heat source. The fully mixed fresh gases are ignited and rapidly turn to burned gases.

In the analysis, the following assumptions are implemented:

- The envisaged frequencies are assumed sufficiently small to consider the combustion zone to be "compact" [1] compared to the acoustic wavelength and to only take into account the longitudinal waves. The acoustic field can thus be described by the superposition of forward and backward propagating plane waves.
- The fluids before and after the combustion zone are assumed to be perfect gases. The temperature T can be expressed as a function of pressure p and density ρ.
- Entropy waves are mainly formed during the unsteady combustion process. Vorticity is neglected in the current analysis.

Now consider weak disturbances induced inside the combustor. Acoustic waves propagate in both directions. The pressure, velocity and density in section j can be expressed as:

[1] although it is possible to implement several staged combustion zones.

$$p_j(x,t) = \bar{p}_j + p'_j(x,t) = \bar{p}_j + A_j^+\left(t-\tau_j^+\right) + A_j^-\left(t-\tau_j^-\right) \tag{1a}$$

$$u_j(x,t) = \bar{u}_j + u'_j(x,t) = \bar{u}_j + \frac{1}{\bar{\rho}_j\bar{c}_j}\left[A_j^+\left(t-\tau_j^+\right) - A_j^-\left(t-\tau_j^-\right)\right] \tag{1b}$$

$$\rho_j(x,t) = \bar{\rho}_j + \rho'_j(x,t) = \bar{\rho}_j + \frac{1}{\bar{c}_j^2}\left[A_j^+\left(t-\tau_j^+\right) + A_j^-\left(t-\tau_j^-\right)\right] - \frac{1}{\bar{c}_j^2}E_j\left(t-\tau_j^s\right) \tag{1c}$$

where A_j^+ and A_j^- denote the amplitude of the downstream and upstream propagating acoustic waves respectively. $E_j = \bar{\rho}_j\bar{c}_j^2/C_{p,j}s'_j$ represents the amplitude of entropy waves. $\tau_j^+ = (x-x_{j-1})\Big/(\bar{c}_j+\bar{u}_j)$, $\tau_j^- = (x_j-x)\Big/(\bar{c}_j-\bar{u}_j)$ and $\tau_j^s = (x-x_{j-1})/\bar{u}_j$ are time delays.

2.1 Without heat addition

2.1.1 Area increase

It is necessary to link the thermal properties and mean flow variables between neighbouring combustor sections. We firstly consider the case without heat addition. At the area increase interface, the mass and energy flux are unchanged, however the momentum flux is increased by the axial force on the walls [6]. We thus have the relations:

$$\Theta_j\rho_{j+1}(x_j,t)u_{j+1}(x_j,t) = \rho_j(x_j,t)u_j(x_j,t) \tag{2a}$$

$$p_{j+1}(x_j,t) + \rho_{j+1}(x_j,t)u_{j+1}^2(x_j,t) = p_j(x_j,t) + \frac{1}{\Theta_j}\rho_j(x_j,t)u_j^2(x_j,t) \tag{2b}$$

$$H_{j+1}(x_j,t) = H_j(x_j,t) \tag{2c}$$

where H is the enthalpy of the flux and $\Theta_j = S_{j+1}/S_j$ denotes the ratio of sectional surface areas. Considering weak disturbances, the high order terms can be neglected and it is possible to write out the stationary and first order term forms to relate the upstream and downstream acoustic waves. The stationary forms of the conservation equations give:

$$\Theta_j\bar{\rho}_{j+1}\bar{u}_{j+1} = \bar{\rho}_j\bar{u}_j \tag{3a}$$

$$\bar{p}_{j+1} + \bar{\rho}_{j+1}\bar{u}_{j+1}^2 = \bar{p}_j + \frac{1}{\Theta_j}\bar{\rho}_j\bar{u}_j^2 \tag{3b}$$

$$\frac{\gamma}{\gamma-1}\left(\Theta_j\bar{p}_{j+1}\bar{u}_{j+1} - \bar{p}_j\bar{u}_j\right) + \frac{1}{2}\bar{\rho}_j\bar{u}_j\left(\bar{u}_{j+1}^2 - \bar{u}_j^2\right) = 0 \tag{3c}$$

The first order forms in the Laplace domain give:

$$\mathcal{B}_{j,2}\begin{bmatrix}\tilde{p}_{j+1}(x_j,s)\\ \bar{\rho}_{j+1}\bar{c}_{j+1}\tilde{u}_{j+1}(x_j,s)\\ \tilde{\rho}_{j+1}(x_j,s)\bar{c}_{j+1}^2\end{bmatrix}=\mathcal{B}_{j,1}\begin{bmatrix}\tilde{p}_{j}(x_j,s)\\ \bar{\rho}_{j}\bar{c}_{j}\tilde{u}_{j}(x_j,s)\\ \tilde{\rho}_{j}(x_j,s)\bar{c}_{j}^2\end{bmatrix} \tag{4}$$

where,

$$\mathcal{B}_{j,1}=\begin{bmatrix}0 & \frac{\bar{c}_{j+1}}{\bar{c}_j} & \bar{M}_j\frac{\bar{c}_{j+1}}{\bar{c}_j}\\ \Theta_j & 2\bar{M}_j & \bar{M}_j^2\\ \frac{\gamma}{\gamma-1}\bar{M}_j & \bar{M}_j^2 & -\frac{1}{\gamma-1}\bar{M}_j\end{bmatrix} \tag{5a}$$

$$\mathcal{B}_{j,2}=\Theta_j\begin{bmatrix}0 & 1 & \bar{M}_{j+1}\\ 1 & 2\bar{M}_{j+1} & \bar{M}_{j+1}^2\\ \frac{\gamma}{\gamma-1}\frac{\bar{c}_{j+1}}{\bar{c}_j}\bar{M}_{j+1} & \frac{\bar{c}_{j+1}}{\bar{c}_j}\bar{M}_{j+1}^2 & -\frac{1}{\gamma-1}\frac{\bar{c}_{j+1}}{\bar{c}_j}\bar{M}_{j+1}\end{bmatrix} \tag{5b}$$

The superscript ˜ indicates the Laplace transform. $s=\sigma+i2\pi f$ represents the Laplace variable, σ is the growth rate and f denotes the frequency.

2.1.2 Area decrease

At an area decrease interface, the mass and energy flux are unchanged. The flow through the area change interface can be assumed isentropic. The momentum equation is replaced by:

$$\frac{p_{j+1}(x_j,t)}{\rho_{j+1}^{\gamma}(x_j,t)}=\frac{p_j(x_j,t)}{\rho_j^{\gamma}(x_j,t)} \tag{6}$$

with its stationary forms:

$$\frac{\bar{p}_{j+1}}{\bar{\rho}_{j+1}^{\gamma}}=\frac{\bar{p}_j}{\bar{\rho}_j^{\gamma}} \tag{7}$$

and the corresponding coefficients of the first order forms in the Laplace domain:

$$\mathcal{B}_{j,1} = \begin{bmatrix} 0 & \frac{\bar{c}_{j+1}}{\bar{c}_j} & \bar{M}_j \frac{\bar{c}_{j+1}}{\bar{c}_j} \\ \frac{1}{\bar{\rho}_j^\gamma} & 0 & -\frac{1}{\bar{\rho}_j^\gamma} \\ \frac{\gamma}{\gamma-1}\bar{M}_j & \bar{M}_j^2 & -\frac{1}{\gamma-1}\bar{M}_j \end{bmatrix} \tag{8a}$$

$$\mathcal{B}_{j,2} = \Theta_j \begin{bmatrix} 0 & 1 & \bar{M}_{j+1} \\ \frac{1}{\Theta_j \bar{\rho}_{j+1}^\gamma} & 0 & -\frac{1}{\Theta_j \bar{\rho}_{j+1}^\gamma} \\ \frac{\gamma}{\gamma-1}\frac{\bar{c}_{j+1}}{\bar{c}_j}\bar{M}_{j+1} & \frac{\bar{c}_{j+1}}{\bar{c}_j}\bar{M}_{j+1}^2 & -\frac{1}{\gamma-1}\frac{\bar{c}_{j+1}}{\bar{c}_j}\bar{M}_{j+1} \end{bmatrix} \tag{8b}$$

2.2 With heat addition

We now consider the case with flame. In general, the flame is located at an area increase interface. We thus can assume that the change of the flow across this interface has two steps: the flow expands at the position of the abrupt area increase and is then heated by the flame. It is thus possible to write out the link of thermal properties and mean flow across the flame.

(i) Expansion:

$$\Theta_j \rho_{j+\frac{1}{2}}(x_j,t) u_{j+\frac{1}{2}}(x_j,t) = \rho_j(x_j,t) u_j(x_j,t) \tag{9a}$$

$$p_{j+\frac{1}{2}}(x_j,t) + \rho_{j+\frac{1}{2}}(x_j,t) u_{j+\frac{1}{2}}^2(x_j,t) = p_j(x_j,t) + \frac{1}{\Theta_j}\rho_j(x_j,t) u_j^2(x_j,t) \tag{9b}$$

$$H_{j+\frac{1}{2}}(x_j,t) = H_j(x_j,t) \tag{9c}$$

(ii) Heat addition:

$$\rho_{j+1}(x_j,t) u_{j+1}(x_j,t) = \rho_{j+\frac{1}{2}}(x_j,t) u_{j+\frac{1}{2}}(x_j,t) \tag{10a}$$

$$p_{j+1}(x_j,t) + \rho_{j+1}(x_j,t) u_{j+1}^2(x_j,t) = p_{j+\frac{1}{2}}(x_j,t) + \rho_{j+\frac{1}{2}}(x_j,t) u_{j+\frac{1}{2}}^2(x_j,t) \tag{10b}$$

$$\rho_{j+1}(x_j,t) u_{j+1}(x_j,t) H_{j+1}(x_j,t) = \rho_{j+\frac{1}{2}}(x_j,t) u_{j+\frac{1}{2}}(x_j,t) H_{j+\frac{1}{2}}(x_j,t) + \dot{q}(t) \tag{10c}$$

$$p_j(x_j,t) = \rho_j(x_j,t) R_{g,1} T_j(x_j,t), \quad p_{j+\frac{1}{2}}(x_j,t) = \rho_{j+\frac{1}{2}}(x_j,t) R_{g,2} T_{j+\frac{1}{2}}(x_j,t) \tag{10d}$$

where $\dot{q}(t)$ denotes the heat release rate per surface area. In general, the temperature ratio across the flame $\bar{T}_{j+1}/\bar{T}_j \approx 5-7$ for hydrocarbon flames and the heat capacity C_p depends on temperature and can not be considered constant. The enthalpy of the flow should thus be expressed as

$$\bar{H} = \int_{\bar{T}_0}^{\bar{T}} C_p \mathrm{d}T + \frac{1}{2}\bar{u}_j^2 \tag{11}$$

where $\bar{T}_0 = 298.15$ K. The heat release rate $\dot{q}$ is from the reaction of the fuel or from the heating grid in case of a Rijke tube. Herein, it is important to note that the heat capacity ratio γ varies across the flame. To simplify the calculation, we use γ_1 and γ_2 to represent the heat capacity ratio in the combustor sections before and after the flame. The determination of the temperature of the reactants and γ_2 are detailed in Appendix A.

2.2.1 Flame model

The flame model describes how fluctuations in the heat release rate, depend on the flow fluctuations induced by the acoustics just ahead of the flame.

Linear flame transfer function

For weak perturbations, the linear flame transfer function (FTF) has been used for decades to describe the linear response of heat release rate perturbations to disturbances in the velocity $\hat{u}$ or the equivalence ratio $\hat{\phi}$. The link can be mathematically expressed in the Laplace-domain:

$$\frac{\tilde{\dot{q}}(s)}{\bar{\dot{q}}} = \widetilde{\mathcal{T}}_u(s)\frac{\tilde{u}(s)}{\bar{u}} + \widetilde{\mathcal{T}}_\phi(s)\frac{\tilde{\phi}(s)}{\bar{\phi}} \tag{12}$$

where $\widetilde{\mathcal{T}}_u(s)$ and $\widetilde{\mathcal{T}}_\phi(s)$ denote the responses of the flame to velocity perturbations $\tilde{u}$ and incoming mixture inhomogeneities $\tilde{\phi}$ respectively. In this work, only the transfer function $\widetilde{\mathcal{T}}_u(s)$ is accounted for. For practical combustion chambers, the impedance of the fuel feed line is generally much larger than that of the air line. When the pressure disturbances interact with the injection unit (fuel+air), only the air line will respond significantly to these disturbances. There is thus a relation between the mixture composition and velocity disturbances which can be expressed as $\tilde{\phi}/\bar{\phi} = -\tilde{u}/\bar{u}$ [7], or $\tilde{\phi}/\bar{\phi} = -k_1\tilde{u}/\bar{u}\Big/(1+k_1\tilde{u}/\bar{u})$ proposed by [8], where k_1 is a coefficient of the mixture strength model. Herein, we can express the normalized heat release rate disturbances as the function of normalized velocity perturbations in the unburned gases:

$$\frac{\tilde{\dot{q}}(s)}{\bar{\dot{q}}} = \mathcal{T}_u(s)\frac{\tilde{u}_u(s)}{\bar{u}_u} \tag{13}$$

where the subscript u denotes unburned gases.

The flame model then describes how the (normalized) unsteady heat release rate of the flame responds to (normalized) velocity fluctuations. One can choose between prescribing a flame transfer function model (with non-linearity options) or loading and fitting experimental data in the operating panel of the OSCILOS. Four kinds of flame transfer function (FTF) models can be prescribed: the first three involve (1) Crocco's famous $n-\tau$ model [9]; (2) the $n-\tau$ model filtered

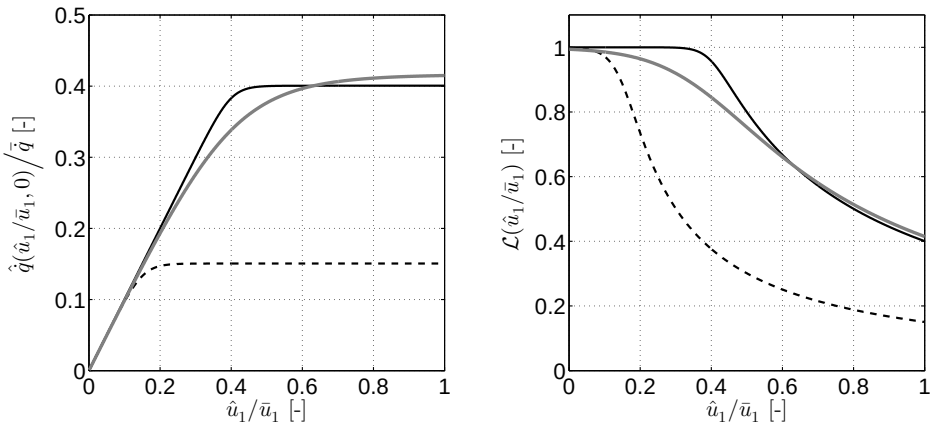

Figure 2: Three examples of the nonlinear model. Black solid line: $\alpha = 0.6$ and $\beta = 40$; gray solid line: $\alpha = 0.6$ and $\beta = 10$; dashed line: $\alpha = 0.85$ and $\beta = 40$ (this model is used in the later calculations).

by a first order filter [10, 11] to capture the flame response shape for conical flames; (3) the $n-\tau$ model filtered by a second order filter [11] to capture the flame response shape for V-shape flames. These FTF models can be expressed as:

$$\mathcal{T}_{u,1}(s) = a_f e^{-\tau_f s} \tag{14a}$$

$$\mathcal{T}_{u,2}(s) = \frac{\omega_c}{s+\omega_c} a_f e^{-\tau_f s} \tag{14b}$$

$$\mathcal{T}_{u,3}(s) = \frac{\omega_c^2}{s^2 + 2\xi\omega_c s + \omega_c^2} a_f e^{-\tau_f s} \tag{14c}$$

where a_f is the gain and τ_f indicates the time delay. $\omega_c = 2\pi f_c$ denotes the cut-off frequency of the filter and ξ represents the damping coefficient of the second order low pass filter.

$$\mathcal{T}_u(s) = \frac{b_1 s^{n-1} + b_2 s^{n-2} + \cdots + b_{n-1}s + b_n}{a_1 s^{m-1} + a_2 s^{m-2} + \cdots + a_{m-1}s + a_m} \tag{15}$$

The fourth option is a user-defined FTF model using a polynomial transfer function, as shown in Eq. 15, by inputting the numerator coefficients **b** and denominator coefficients **a**. The order of the numerator should not be larger than that of denominator $n \leq m$.

Nonlinear flame describing function

In practice, most flames feature a nonlinear response to flow disturbances [12, 13, 14, 15, 16]. Saturation of the heat release rate amplitude or a phase lag change relative to the acoustic pressure (and hence a change in the Rayleigh source term $< p'\dot{q}' >$ driving combustion instabilities [17, 18]) with the modulation level have been experimentally identified in many cases [19, 20, 15, 21].

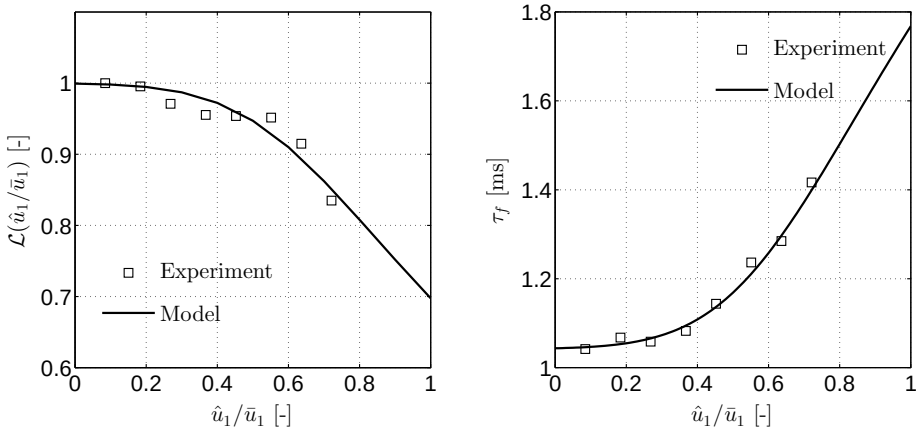

Figure 3: Comparison between the experimental results from Fig. 7 in [22] and t he nonlinear model ($\alpha = 0.3$, $\beta = 6$ and $\tau_f^N = 2.4$ ms). Left figure: $f = 400$ Hz, $\mathcal{L}(\hat{u}_1/\bar{u}_1) = |\widetilde{G}(\hat{u}_1/\bar{u}_1, f)| \Big/ |\widetilde{G}(0, f)|$. Right figure: τ_f is calculated by linear fitting of the phase for modulating frequency ranging from 0 Hz to 600 Hz.

It is clear that the linear flame transfer function is not enough to anticipate all of the characteristics of combustion instabilities; in particular it cannot predict the saturation amplitude or the time to limit cycle. The concept of a "flame describing function" (FDF) has been proposed, treating the response of heat release rate as a linear regime for small perturbation levels and a weakly nonlinear regime for larger disturbance amplitudes [11, 20].

In OSCILOS, users can choose between prescribing an analytically nonlinear flame describing function or loading and fitting experimental / CFD data. Two kinds of nonlinear flame describing functions can be prescribed: (1) an abrupt heat release rate ratio $\hat{\dot{q}}/\bar{\dot{q}}$ saturation model proposed by Dowling [11], which can be mathematically expressed as:

$$\frac{\dot{q}'}{\bar{\dot{q}}} = \begin{cases} \left(\dfrac{\dot{q}'}{\bar{\dot{q}}}\right)_L & \text{for } \left|\dfrac{\dot{q}'}{\bar{\dot{q}}}\right| \le \alpha \\ \alpha \ \mathrm{sgn}\left(\dfrac{\dot{q}'}{\bar{\dot{q}}}\right) & \text{else} \end{cases} \tag{16}$$

where α is a constant associated with the saturation ($0 \le \varphi \le 1$) and $\left(\dot{q}' \Big/ \bar{\dot{q}}\right)_L$ denotes the heat release rate ratio for weak perturbations, which can be calculated from the linear flame transfer function.

(2) The second nonlinear model is recently proposed by the authors [24]. The nonlinear flame describing function depends on s and velocity ratio $\hat{u}_1/\bar{u}_1$ and it is assumed here can be decoupled as:

$$\widetilde{G}(\hat{u}_1/\bar{u}_1, s) = \mathcal{L}(\hat{u}_1/\bar{u}_1)\widetilde{\mathcal{T}}_u(s) \tag{17}$$

where the superscript $\hat{}$ indicates the signal amplitude. The nonlinear function $\mathcal{L}(\hat{u}_1/\bar{u}_1)$ describes the saturation of heat release rate with velocity perturbations $\hat{u}_1/\bar{u}_1$, and $\mathcal{L}(\hat{u}_1/\bar{u}_1) = \widetilde{G}(\hat{u}_1/\bar{u}_1, 0)$. The mathematical link proposed in [24] is:

$$\frac{\widehat{\dot{q}}(\hat{u}_1/\bar{u}_1, 0)}{\bar{\dot{q}}} = \mathcal{L}(\hat{u}_1/\bar{u}_1)\frac{\hat{u}_1}{\bar{u}_1} = \int_0^{\hat{u}_1/\bar{u}_1} \frac{1}{1 + \big(\xi + \alpha\big)^{\beta}} \mathrm{d}\xi \tag{18}$$

where α and β are two coefficients which determine the shape of the nonlinear model. Figure 2 shows 3 examples of the proposed nonlinear model. The left figure shows the evolution of heat release rate perturbation ratio $\widehat{\dot{q}}/\bar{\dot{q}}$ with velocity disturbance level $\hat{u}_1/\bar{u}_1$ when $s = 0$, while the trajectories of the nonlinear function $\mathcal{L}$ are presented in the right figure. For weak velocity disturbances, the link between $\widehat{\dot{q}}/\bar{\dot{q}}$ and $\hat{u}_1/\bar{u}_1$ is linear. For example, the linear region for the first case is $\hat{u}_1/\bar{u}_1 \in$[0 0.4], with corresponding proportional coefficient $\mathcal{L} \approx 1$ in the right figure. One may denote the upper limit of the linear region by the velocity disturbance ratio $\big(\hat{u}_1/\bar{u}_1\big)_s$. When the level of velocity disturbances exceeds $\big(\hat{u}_1/\bar{u}_1\big)_s$, $\mathcal{L}$ decreases and the heat release rate perturbations begin to saturate. It can be found that the saturation limit $\big(\hat{u}_1/\bar{u}_1\big)_s$ is mainly determined by the coefficient α; $\big(\hat{u}_1/\bar{u}_1\big)_s$ decreases as α increases towards unity. The smoothness of the saturation corner is controlled by the coefficient β. The proposed model guarantees saturation for larger velocity perturbation ratios.

One may also introduce a simple nonlinear model of the time delay, using the mathematical description:

$$\tau_f = \tau_f^0 + \tau_f^N\big(1 - \mathcal{L}(\hat{u}_1/\bar{u}_1)\big) \tag{19}$$

where τ_f^0 means the time delay when $\hat{u}_1/\bar{u}_1 = 0$ and τ_f^N is a time delay to describe the change of τ_f as $\mathcal{L}$ changes.

Figure 3 shows the comparison between the experimental matrix burner measurements and the nonlinear model. A good match is found for the evolutions of gain and time delay of the flame describing function with the increase of velocity disturbances. The exact form of the nonlinear flame model is not fully representative of a real configuration, but provides a simplified model which captures nonlinear features of real experimental flames significantly better than a simple $n - \tau$ model with abrupt saturation [25, 26] as shown in Figure 3, and thus can be used to get a better understanding of combustion instabilities.

The first order expressions linking the fresh mixture and burned gases after the flame can be written as:

$$\mathcal{B}^{\mathrm{ii}}_{j,2}\begin{bmatrix} \tilde{p}_{j+1}(x_j, s) \\ \bar{\rho}_{j+1}\bar{c}_{j+1}\tilde{u}_{j+1}(x_j, s) \\ \tilde{\rho}_{j+1}(x_j, s)\bar{c}^2_{j+1} \end{bmatrix} = \mathcal{B}^{\mathrm{ii}}_{j,1a}\begin{bmatrix} \tilde{p}_{j+\frac{1}{2}}(x_j, s) \\ \bar{\rho}_{j+\frac{1}{2}}\bar{c}_{j+\frac{1}{2}}\tilde{u}_{j+\frac{1}{2}}(x_j, s) \\ \tilde{\rho}_{j+\frac{1}{2}}(x_j, s)\bar{c}^2_j \end{bmatrix} + \mathcal{B}^{\mathrm{ii}}_{j,1b}\begin{bmatrix} \tilde{p}_j(x_j, s) \\ \bar{\rho}_j\bar{c}_j\tilde{u}_j(x_j, s) \\ \tilde{\rho}_j(x_j, s)\bar{c}^2_j \end{bmatrix} \tag{20a}$$

$$\mathcal{B}^{\mathrm{i}}_{j,2}\begin{bmatrix} \tilde{p}_{j+\frac{1}{2}}(x_j, s) \\ \bar{\rho}_{j+\frac{1}{2}}\bar{c}_{j+\frac{1}{2}}\tilde{u}_{j+\frac{1}{2}}(x_j, s) \\ \tilde{\rho}_{j+\frac{1}{2}}(x_j, s)\bar{c}^2_j \end{bmatrix} = \mathcal{B}^{\mathrm{i}}_{j,1}\begin{bmatrix} \tilde{p}_j(x_j, s) \\ \bar{\rho}_j\bar{c}_j\tilde{u}_j(x_j, s) \\ \tilde{\rho}_j(x_j, s)\bar{c}^2_j \end{bmatrix} \tag{20b}$$

where,

$$\mathcal{B}^{\text{ii}}_{j,2} = \begin{bmatrix} 0 & 1 & \bar{M}_{j+1} \\ 1 & 2\bar{M}_{j+1} & \bar{M}^2_{j+1} \\ \dfrac{\gamma_2}{\gamma_2-1}\dfrac{\bar{c}_{j+1}}{\bar{c}_{j+\frac{1}{2}}}\bar{M}_{j+1} & \dfrac{\bar{c}_{j+1}}{\bar{c}_{j+\frac{1}{2}}}\bar{M}^2_{j+1} & -\dfrac{1}{\gamma_2-1}\dfrac{\bar{c}_{j+1}}{\bar{c}_{j+\frac{1}{2}}}\bar{M}_{j+1} \end{bmatrix} \tag{21a}$$

$$\mathcal{B}^{\text{ii}}_{j,1a} = \begin{bmatrix} 0 & \dfrac{\bar{c}_{j+1}}{\bar{c}_{j+\frac{1}{2}}} & \bar{M}_{j+\frac{1}{2}}\dfrac{\bar{c}_{j+1}}{\bar{c}_{j+\frac{1}{2}}} \\ 1 & 2\bar{M}_{j+\frac{1}{2}} & \bar{M}^2_{j+\frac{1}{2}} \\ \dfrac{\gamma_1}{\gamma_1-1}\bar{M}_{j+\frac{1}{2}} & \bar{M}^2_{j+\frac{1}{2}} - \dfrac{\Delta H}{\bar{c}^2_{j+\frac{1}{2}}} & -\bar{M}_{j+\frac{1}{2}}\Big(\dfrac{1}{\gamma_1-1} + \dfrac{\Delta H}{\bar{c}^2_{j+\frac{1}{2}}}\Big) \end{bmatrix} \tag{21b}$$

$$\mathcal{B}^{\text{ii}}_{j,1b} = \begin{bmatrix} 0 & 0 & 0 \\ 0 & 0 & 0 \\ 0 & \dfrac{\Delta H}{\Theta_j \bar{c}_j \bar{c}_{j+\frac{1}{2}}}\widetilde{\mathcal{G}}_u & 0 \end{bmatrix} \tag{21c}$$

$$\mathcal{B}^{\mathrm{i}}_{j,2} = \Theta_j \begin{bmatrix} 0 & 1 & \bar{M}_{j+\frac{1}{2}} \\ 1 & 2\bar{M}_{j+\frac{1}{2}} & \bar{M}^2_{j+\frac{1}{2}} \\ \dfrac{\gamma_1}{\gamma_1-1}\dfrac{\bar{c}_{j+\frac{1}{2}}}{\bar{c}_j}\bar{M}_{j+\frac{1}{2}} & \dfrac{\bar{c}_{j+\frac{1}{2}}}{\bar{c}_j}\bar{M}^2_{j+\frac{1}{2}} & -\dfrac{1}{\gamma_1-1}\dfrac{\bar{c}_{j+\frac{1}{2}}}{\bar{c}_j}\bar{M}_{j+\frac{1}{2}} \end{bmatrix} \tag{22a}$$

$$\mathcal{B}^{\mathrm{i}}_{j,1} = \begin{bmatrix} 0 & \dfrac{\bar{c}_{j+\frac{1}{2}}}{\bar{c}_j} & \bar{M}_j\dfrac{\bar{c}_{j+\frac{1}{2}}}{\bar{c}_j} \\ \Theta_j & 2\bar{M}_j & \bar{M}^2_j \\ \dfrac{\gamma_1}{\gamma_1-1}\bar{M}_j & \bar{M}^2_j & -\dfrac{1}{\gamma_1-1}\bar{M}_j \end{bmatrix} \tag{22b}$$

Equation 20 can be changed to:

$$\mathcal{B}^{\mathrm{ii}}_{j,2}\begin{bmatrix} \tilde{p}_{j+1}(x_j,s) \\ \bar{\rho}_{j+1}\bar{c}_{j+1}\tilde{u}_{j+1}(x_j,s) \\ \tilde{\rho}_{j+1}(x_j,s)\bar{c}^2_{j+1} \end{bmatrix} = \left(\mathcal{B}^{\mathrm{ii}}_{j,1a}\left(\mathcal{B}^{\mathrm{i}}_{j,2}\right)^{-1}\mathcal{B}^{\mathrm{i}}_{j,1} + \mathcal{B}^{\mathrm{ii}}_{j,1b}\right)\begin{bmatrix} \tilde{p}_j(x_j,s) \\ \bar{\rho}_j\bar{c}_j\tilde{u}_j(x_j,s) \\ \tilde{\rho}_j(x_j,s)\bar{c}^2_j \end{bmatrix} \tag{23}$$

In case there is no area change at the flame position, $\left(\mathcal{B}^{\mathrm{i}}_{j,2}\right)^{-1}\mathcal{B}^{\mathrm{i}}_{j,1} = \mathbf{I}_3$, where $\mathbf{I}_3$ is an dentity matrix.

The array of linearised flow variables $\tilde{p}(s)$, $\bar{\rho}\bar{c}\tilde{u}(s)$ and $\tilde{\rho}(s)\bar{c}^2$ can be expressed as the function of the wave strengths $\widetilde{A}^+$, $\widetilde{A}^-$ and $\widetilde{E}$:

$$\begin{bmatrix} \tilde{p}_{j+1}(x_j,s) \\ \bar{\rho}_{j+1}\bar{c}_{j+1}\tilde{u}_{j+1}(x_j,s) \\ \tilde{\rho}_{j+1}(x_j,s)\bar{c}^2_{j+1} \end{bmatrix} = \mathcal{C}_2\mathcal{D}_{j,2}(s)\begin{bmatrix} \widetilde{A}^+_{j+1}(s) \\ \widetilde{A}^-_{j+1}(s) \\ \widetilde{E}_{j+1}(s) \end{bmatrix} \tag{24a}$$

$$\begin{bmatrix} \tilde{p}_j(x_j,s) \\ \bar{\rho}_j\bar{c}_j\tilde{u}_j(x_j,s) \\ \tilde{\rho}_j(x_j,s)\bar{c}^2_j \end{bmatrix} = \mathcal{C}_1\mathcal{D}_{j,1}(s)\begin{bmatrix} \widetilde{A}^+_j(s) \\ \widetilde{A}^-_j(s) \\ \widetilde{E}_j(s) \end{bmatrix} \tag{24b}$$

where

$$\mathcal{C}_1 = \mathcal{C}_2 = \begin{bmatrix} 1 & 1 & 0 \\ 1 & -1 & 0 \\ 1 & 1 & -1 \end{bmatrix} \tag{25}$$

$$\mathcal{D}_{j,1}(s) = \begin{bmatrix} e^{-\tau_j^+ s} & & \\ & 1 & \\ & & e^{-\tau_j^s s} \end{bmatrix} \qquad \mathcal{D}_{j,2}(s) = \begin{bmatrix} 1 & & \\ & e^{-\tau_{j+1}^- s} & \\ & & 1 \end{bmatrix} \tag{26}$$

Thus:

$$\begin{bmatrix} \widetilde{A}_{j+1}^+(s) \\ \widetilde{A}_{j+1}^-(s) \\ \widetilde{E}_{j+1}(s) \end{bmatrix} = \mathcal{Z}_j(s) \begin{bmatrix} \widetilde{A}_j^+(s) \\ \widetilde{A}_j^-(s) \\ \widetilde{E}_j(s) \end{bmatrix} \tag{27}$$

where

$$\mathcal{Z}_j(s) = \Big(\mathcal{D}_{j,2}(s)\Big)^{-1} \Big(\mathcal{B}_{j,2}\mathcal{C}_2\Big)^{-1} \mathcal{B}_{j,1}\mathcal{C}_1\mathcal{D}_{j,1}(s) \tag{28}$$

The global matrix $\mathcal{G}_{j,k}$ integrates all interfaces from k to j:

$$\mathcal{G}_{k,j}(s) = \mathcal{Z}_j(s)\mathcal{Z}_{j-1}(s)\ldots\mathcal{Z}_k(s) \tag{29}$$

The link between magnitudes of the acoustic waves and entropy waves at the inlet of the combustor ($\widetilde{A}_1^+(s)$, $\widetilde{A}_1^-(s)$ and $\widetilde{E}_1(s)$) and those at the outlet ($\widetilde{A}_N^+(s)$, $\widetilde{A}_N^-(s)$ and $\widetilde{E}_N(s)$) can be expressed as:

$$\begin{bmatrix} \widetilde{A}_N^+(s) \\ \widetilde{A}_N^-(s) \\ \widetilde{E}_N(s) \end{bmatrix} = \mathcal{G}_{1,N-1}(s) \begin{bmatrix} \widetilde{A}_1^+(s) \\ \widetilde{A}_1^-(s) \\ \widetilde{E}_1(s) \end{bmatrix} \tag{30}$$

2.2.2 Advection of entropy waves

For low Mach number situations, the entropy waves vary rapidly along the longitudinal direction and hence are likely to undergo shear dispersion in long chambers. We thus account for the attenuation of the entropy waves over the long chamber and $\mathcal{C}_1$ can be changed to:

$$\mathcal{C}_1 = \begin{bmatrix} 1 & 1 & 0 \\ 1 & -1 & 0 \\ 1 & 1 & 0 \end{bmatrix} \tag{31}$$

For large Mach number situations, at the combustor exit (choked end) / turbine inlet, the entropy waves are subjected to a rapid flow acceleration due to the significant cross sectional area convergence, and this results in the generation of acoustic waves, as first described by [28]. These

acoustic waves are termed 'entropy noise' or 'indirect combustion noise'. The upstream-propagating component affects the flame within the combustor, and thus can influence thermoacoustic stability [29, 7]. Between the flame, where they are generated, and the combustor exit/turbine inlet, where they are accelerated, entropy waves are subject to advection by a flow that has both a non-uniform mean spatial profile (for example, a fully developed profile) and turbulent fluctuations. Two models accounting for the advection of entropy waves are prescribed in this work. These models considered the impulse response at locations downstream of the flame within a combustor. The impulse response is the time variation of the entropy perturbation (averaged over cross-section) that arises from an impulse, $\delta(t)$, applied at the combustor inlet, nominally the flame location. This corresponds to the probability density function (p.d.f.) of the 'residence time' of a particle advecting from the inlet to the outlet. The model options for the shear dispersion effects are:

- A "Rectangular" model (proposed by Sattelmayer [30]): The p.d.f. or impulse response is modelled as a rectangular pulse of length $2\Delta\tau_C^s$ and height $1/2\Delta\tau_C^s$ centred about the mean residence time τ_C^s:

$$E_C^{\text{inlet}}(t) = \delta(t) \tag{32a}$$

$$E_C^{\text{outlet}}(t) = \begin{cases} \dfrac{1}{2\Delta\tau_C^s} & \text{for } \tau_C^s - \Delta\tau_C^s \leq t \leq \tau_C^s + \Delta\tau_C^s \\ 0 & \text{else} \end{cases} \tag{32b}$$

  The corresponding Laplace transform of the transfer function between the entropy waves at the outlet and inlet can be expressed as:

$$\frac{\widetilde{E}_C^{\text{outlet}}(s)}{\widetilde{E}_C^{\text{inlet}}(s)} = \widetilde{\mathcal{E}}(s)\exp\big(-\tau_C^s\ s\big) = \frac{\exp\big(\Delta\tau_C^s\ s\big) - \exp\big(-\Delta\tau_C^s\ s\big)}{2\Delta\tau_C^s\ s}\exp\big(-\tau_C^s\ s\big) \tag{33}$$

  with the Fourier transforms of the transfer function:

$$\widetilde{\mathcal{E}}(i\omega) = \text{sinc}\big(i\omega\Delta\tau_C^s\big) \tag{34}$$

  where the function $\text{sinc}(x) = \sin(x)/x$.

- A "Gaussian" model (proposed by Morgans et al. [31]): Shear dispersion is assumed to be predominantly caused by spatial variations in the time-mean velocity profile, rather than by turbulent eddies. DNS simulations of a channel flow show that the p.d.f. exhibits a Gaussian-like shape with extended back-foot. The impulse response is modelled as a Gaussian distribution:

$$E_C^{\text{inlet}}(t) = \delta(t) \tag{35a}$$

$$E_C^{\text{outlet}}(t) = A_\delta \exp\Big(-\pi A_\delta^2\big(t-\tau_C^s\big)^2\Big) \tag{35b}$$

  A time delay $\Delta\tau_C^s$ is also proposed to describe the dispersion of resident time using the definition:

$$E_C^{\text{outlet}}(\tau_C^s + \Delta\tau_C^s) = A_\delta \exp\Big(-\pi A_\delta^2\big(\Delta\tau_C^s\big)^2\Big) = A_\delta\exp(-1) \tag{36}$$

A_δ thus can be expressed as the function of $\Delta\tau_C^s$:

$$A_\delta = \frac{1}{\sqrt{\pi}\Delta\tau_C^s} \tag{37}$$

Equation 35b can be changed to:

$$E_C^{\text{outlet}}(t) = \frac{1}{\sqrt{\pi}\Delta\tau_C^s} \exp\left(-\left(\frac{t-\tau_C^s}{\Delta\tau_C^s}\right)^2 \right) \tag{38}$$

with the Fourier transforms of the transfer function:

$$\widetilde{\mathcal{E}}(i\omega) = \exp\left(-\frac{\left(\omega\Delta\tau_C^s\right)^2}{4} \right) \tag{39}$$

For causal systems, the Fourier and Laplace transforms are the same and the above Fourier transform are changed to the Laplace transform by replacing $i\omega$ by the Laplace variable s, which yields:

$$\widetilde{\mathcal{E}}(s) = \exp\left(\frac{\left(\Delta\tau_C^s\ s\right)^2}{4} \right) \tag{40}$$

The coefficient $\mathcal{D}_{j,1}(s)$ in the combustor section in this situation thus should be changed to:

$$\mathcal{D}_{C,1}(s) = \begin{bmatrix} e^{-\tau_C^+ s} & & \\ & 1 & \\ & & k_d\widetilde{\mathcal{E}}(s)e^{-\tau_C^s s} \end{bmatrix} \tag{41}$$

where $k_d \leq 1$, is a dissipative factor to account for the fact that the integrated strength of an entropy wave is reduced [7].

3 Boundary conditions

The link between the outward and inward propagating waves at the end of the combustor can be described by the reflection coefficients. When the indirect noise induced by the entropy waves can be neglected, the pressure reflection coefficients at the inlet and outlet are characterized by R_1 and R_2 respectively:

$$\widetilde{R}_1(s) = \frac{\widetilde{A}_1^+(s)}{\widetilde{A}_1^-(s)e^{-\tau_1^- s}} \tag{42a}$$

$$\widetilde{R}_2(s) = \frac{A_N^-(s)}{A_N^+(s)e^{-\tau_N^+ s}} \tag{42b}$$

The compressor exit and turbine inlet of a gas turbine or an aeronautic engine can be considered as a choked inlet and choked outlet respectively. The sections before and after the choked interface can be considered as independent systems. One can treat the choked interface as a boundary for the analysis of instabilities.

- Compact choked inlet: Stow et al. [32] found that for one-dimensional disturbances, perturbations in mass flux and energy flux are zero just after the shock and we have the mathematical expressions:

$$\rho_1' \bar{c}_1^2 + \frac{\bar{\rho}_1 \bar{c}_1 u_1'}{\bar{M}_1} = 0 \tag{43a}$$

$$\frac{\gamma_1 p_1'}{\gamma_1 - 1} - \frac{\rho_1' \bar{c}_1^2}{\gamma_1 - 1} + \bar{M}_1 \bar{\rho}_1 \bar{c}_1 u_1' = 0 \tag{43b}$$

  The reflection coefficients can be obtained by combining the above two equations:

$$\widetilde{R}_1(s) = \frac{1 - \gamma_1 \bar{M}_1 / \left(1 + (\gamma_1 - 1)\bar{M}_1^2\right)}{1 + \gamma_1 \bar{M}_1 / \left(1 + (\gamma_1 - 1)\bar{M}_1^2\right)} \tag{44}$$

- Compact choked outlet: Marble and Candel [28] showed that the boundary condition at a compact choked outlet can be expressed as:

$$\rho_N' \bar{c}_N^2 + \frac{2\bar{\rho}_N \bar{c}_N u_N'}{\bar{M}_N} - \gamma_2 p_N' = 0 \tag{45}$$

  which can be simplified to the function of $\widetilde{A}_N^+$, $\widetilde{A}_N^-$ and $\widetilde{E}_N$:

$$\widetilde{A}_N^-(s) = \widetilde{R}_2(s)\widetilde{A}_N^+(s)\exp(-\tau_N^+ s) + k_d \widetilde{R}_s(s)\widetilde{E}_N(s)\widetilde{\mathcal{E}}(s)\exp(-\tau_N^s s) \tag{46a}$$

$$\widetilde{R}_2(s) = \frac{1 - (\gamma_2 - 1)\bar{M}_N/2}{1 + (\gamma_2 - 1)\bar{M}_N/2} \tag{46b}$$

$$\widetilde{R}_s(s) = -\frac{\bar{M}_N/2}{1 + (\gamma_2 - 1)\bar{M}_N/2} \tag{46c}$$

Users can also define the reflection coefficient as a polynomial transfer function, as shown in Eq. 47, by inputting the numerator coefficients **b** and denominator coefficients **a**. The order of the numerator should not be larger than that of denominator $n \leq m$.

$$\widetilde{R}(s) = \frac{b_1 s^{n-1} + b_2 s^{n-2} + \cdots + b_{n-1}s + b_n}{a_1 s^{m-1} + a_2 s^{m-2} + \cdots + a_{m-1}s + a_m} \tag{47}$$

4 Validation of the code

Validation of the code has been carried out for two cases. The first case is a cold tube without heat addition and the second one is an unstable laboratory combustor.

4.1 Cold tube without heat addition

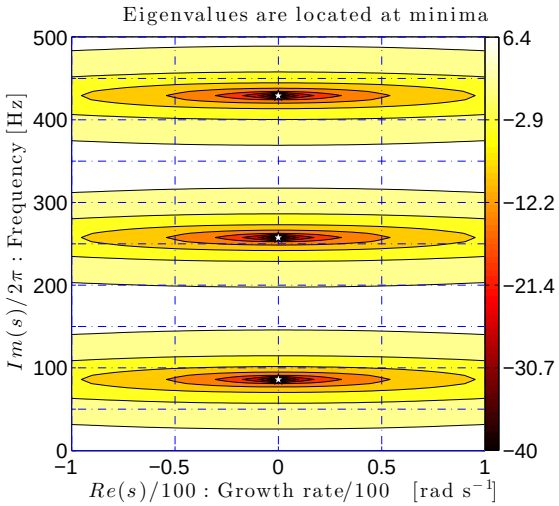

Figure 4: Contour map of $20\log_{10}|\delta e(s)|$ in the s-plane. The first three resonant frequencies indicated by the marker $\star$ are 85.8 Hz, 257.4 Hz and 429.1 Hz respectively.

It is worth firstly discussing the situation without heat addition, such that the thermodynamic properties in the tube are uniform and we solve for the purely acoustic (rather than thermoacoustic) modes. The tube has a length of $l = 1$ m. The mean pressure, temperature and Mach number in the tube are $\bar{p} = 1$ bar, $\overline{T} = 300$ K and $\bar{M} = 0.001$. The inlet of the tube is a rigid wall (i.e. a closed end) and the outlet is open to the atmosphere and radiation at the end is neglected. The pressure reflection coefficients at the inlet and outlet are $R_1 = 1$ and $R_2 = -1$ respectively, which corresponds to:

$$u'(0,t) = 0 \tag{48a}$$

$$p'(l,t) = 0 \tag{48b}$$

The theoretical resonant frequency can be found from the following equation [6]:

$$\cos(2\pi f l/\bar{c}) = 0 \tag{49}$$

with solutions:

$$f_n = \frac{2n-1}{4}\frac{\bar{c}}{l} \tag{50}$$

for integer $n \geq 1$. The first three resonant frequencies are 85.8 Hz, 257.4 Hz and 429.1 Hz respectively by substituting the mean speed of sound $\bar{c} = 343.25$ m/s into the above equation. Moreover, it also possible to deduce the corresponding mode shapes:

$$\hat{p}(x) = P_n \cos\big((2n-1)\pi x/(2l)\big) \tag{51a}$$

$$\hat{u}(x) = iP_n/(\bar{\rho}\bar{c}) \sin\big((2n-1)\pi x/(2l)\big) \tag{51b}$$

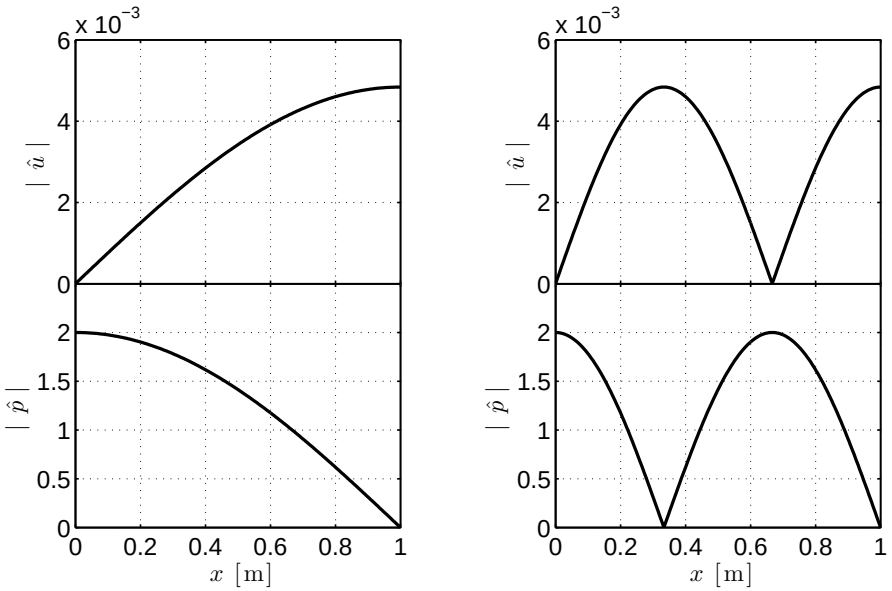

Figure 5: Plots of the mode shapes of the first and second modes.

for an arbitrary constant P_n.

In OSCILOS, we set $\widetilde{A}_1^-(s) = 1$ and $\widetilde{E}_1(s) = 0$ at the inlet of the combustor. To satisfy the boundary condition, $\widetilde{A}_1^+(s) = \widetilde{R}_1(s)\widetilde{A}_1^-(s)\exp(-\tau_1^+ s)$. By guessing a Laplace variable s, we can calculate the values of $\widetilde{A}_N^+(s)e^{-\tau_N^+ s}$, $\widetilde{A}_N^-(s)$ and $\widetilde{E}_N(s)e^{-\tau_N^s s}$ from the equation 30. The error at the outlet boundary can be mathematically expressed as:

$$\delta e(s) = \widetilde{A}_N^-(s) - \widetilde{R}_2(s)\widetilde{A}_N^+(s)\exp(-\tau_N^+ s) - k_d\widetilde{R}_s(s)\widetilde{E}_N(s)\widetilde{\mathcal{E}}(s)\exp(-\tau_N^s s) \tag{52}$$

It is possible to plot the contour map of $20\log_{10}|\delta e(s)|$ (as shown in Fig 4), in which the eigenvalues are located at minima. The resonant frequencies obtained from OSCILOS are the same as those from theoretical prediction. Once the eigenvalues are determined, the mode shapes can be also obtained from OSCILOS. Figure 5 shows the mode shapes of the first two modes. These plots still match well with those predicted from eqs 51a and 51b.

4.2 Unstable laboratory combustor

We now consider the case with an unstable flame. The experiments were carried out by Palies and co-workers in Laboratory EM2C [33]. The combustor can be simplified to three cavities, including a plenum, an injection unit and a combustion chamber terminated by an open end. The compact flame is stabilized at the beginning of the combustion chamber. Experiments were carried out for the plenum and chamber with different lengths to vary the eigenvalues of the combustor. Herein, we only take one unstable case for the comparison between the calculation results from OSCILOS

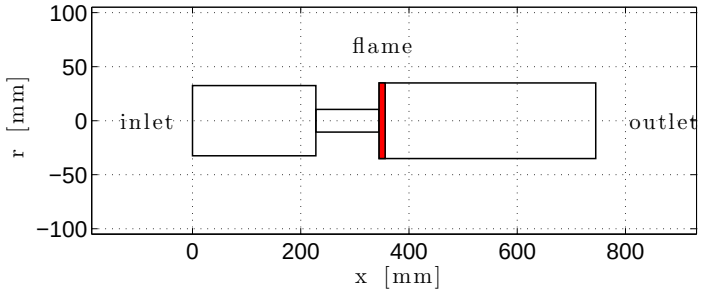

Figure 6: Schematic view of the combustor.

and the experimental results. The lengths of the three sections are 228 mm, 117 mm and 400 mm respectively; corresponding radii are 32.5 mm, 10.5 mm and 35 mm respectively. The mean velocity at the outlet of the injection unit is $\bar{u}_2 = 4.13$ m/s. The mean pressure is $\bar{p}_1 = 1$ bar and the mean temperature is $\overline{T}_1 = 300$ K. Methane is used as the fuel and the equivalence ratio is $\phi = 0.7$. The measured mean temperature of the burned gases is 1600 K. So that the calculated mean temperature matches the experimental result, the combustion efficiency η is set equal to 0.825. It is thus possible to calculate the mean thermal properties and mean flows in different sections. Figure 7 shows the plots of the mean velocity $\bar{u}$ and mean temperature $\overline{T}$ in different sections. $\overline{T}_3 = 1601$ K and $\overline{T}_1 = \overline{T}_2 = 300$ K. The inlet can be considered as a rigid wall and $R_1 = 1$. The outlet of the combustion chamber is open to atmosphere. The flame transfer functions are loaded from the experimental results. A fitting procedure is necessary prior to substituting the flame model into OSCILOS. Figure 8 shows the comparison of the experimental and fitted

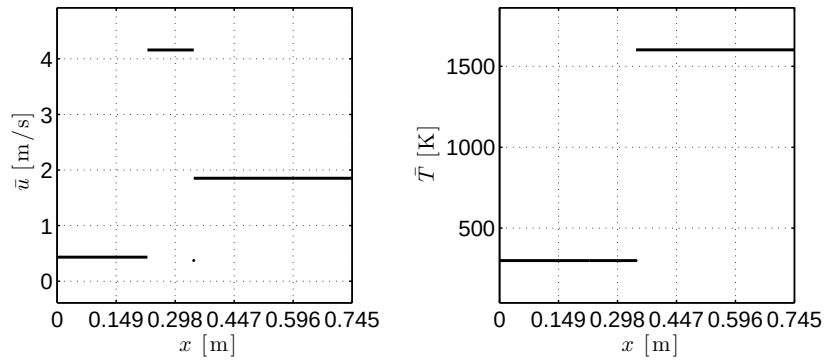

Figure 7: Plots of the mean velocity $\bar{u}$ (left figure) and the mean temperature $\bar{T}$ (right figure) in different sections.

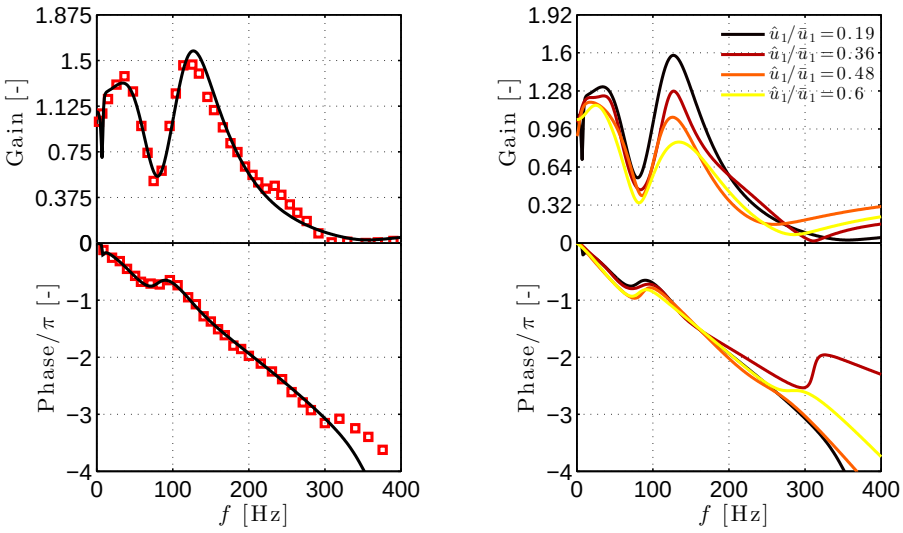

Figure 8: Left figure: comparison of the experimental (markers) and fitted (continuous line) flame transfer function when $\hat{u}_2/\bar{u}_2 = 0.19$. Right figure: plots of fitted FDF for different normalized velocity ratios.

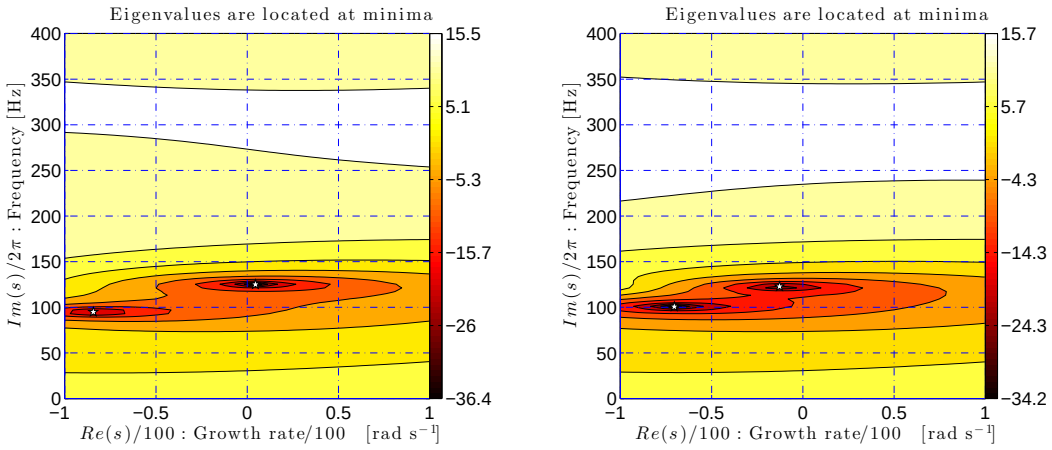

Figure 9: Contour map of $20\log_{10}|\delta e(s)|$ in the s-plane when $\hat{u}_2/\bar{u}_2 = 0.19$ (left figure) and $\hat{u}_2/\bar{u}_2 = 0.36$ (right figure).

flame describing function. The fitted result captures the shape of FDF for the most "dangerous" frequency range (100 - 150 Hz) where combustion instability may occur. By substituting the FDF for different normalized velocity perturbations, one can obtain the evolutions of the eigenvalues with the increase of velocity perturbations. Figure 9 shows the contour maps of $20\lg|\delta e(s)|$ in the s-plane for two velocity perturbations. The eigenvalue with a frequency of 124.9 Hz is on the right side of s-plane indicating that the system is unstable. The predicted resonant frequency is nearly the same as that (126 Hz) measured in the experiment. With the increase of velocity perturbations, the eigenvalue of this mode moves to the left side of s-plane revealing that the system becomes stable and a limit cycle is established. In the experiment, the limit cycle is established when $\hat{u}_2/\bar{u}_2 = 0.48$, which is larger than that predicted by OSCILOS ($\hat{u}_2/\bar{u}_2 = 0.36$). The difference is likely to be due to the difference in the combustor outlet boundary condition.

Appendix A: calculation of adiabatic temperature at dissociation equilibrium

A simple method is presented in this section to calculate the mass fractions of the species of hydrocarbon flame at dissociation equilibrium. To simplify the analysis, we only account for the major species and the products are assumed to be CO_2, CO, H_2O, H_2, O_2 and N_2 for hydrocarbon-air combustion. The species CO_2 and H_2O dissociate at high temperature, even for lean mixture conditions [34]. We assume an ε_1 amount of CO_2 and an ε_2 amount of H_2O dissociations, and the chemical reaction can be written as:

$$\begin{aligned} C_xH_y + a(O_2 + 3.76N_2) \rightarrow & (1-\varepsilon_1)xCO_2 + \varepsilon_1 xCO \\ & + \frac{(1-\varepsilon_2)y}{2}H_2O + \frac{\varepsilon_2 y}{2}H_2 \\ & + \Big((1-\phi)a + \frac{\varepsilon_1 x}{2} + \frac{\varepsilon_2 y}{4}\Big)O_2 + 3.76aN_2 \end{aligned} \tag{53}$$

where $a = (x + y/4)\Big/\phi$. The equilibrium constants for the dissociations of CO_2 and H_2O are:

$$K_{p,1} = \frac{(p_{CO}/p_0)(p_{O_2}/p_0)^{\frac{1}{2}}}{p_{CO_2}/p_0} = \frac{\varepsilon_1 b^{\frac{1}{2}}}{1-\varepsilon_1}\Big(\frac{p}{p_0}\Big)^{\frac{1}{2}} \tag{54}$$

$$K_{p,2} = \frac{(p_{H_2}/p_0)(p_{O_2}/p_0)^{\frac{1}{2}}}{p_{H_2O}/p_0} = \frac{\varepsilon_2 b^{\frac{1}{2}}}{1-\varepsilon_2}\Big(\frac{p}{p_0}\Big)^{\frac{1}{2}} \tag{55}$$

$$b = \frac{(1-\phi)a + \frac{\varepsilon_1 x}{2} + \frac{\varepsilon_2 y}{4}}{x + \frac{y}{2} + (4.76-\phi)a + \frac{\varepsilon_1 x}{2} + \frac{\varepsilon_2 y}{4}} \tag{56}$$

Where p_0 denotes the standard-state pressure and p indicates local ambient pressure. For convenience, we set $p = p_0$. Using the trial-and-error method to determine the adiabatic temperature shown in [34](chapter 1, pages 68 - 90), one can obtain the mass fractions of the product constituents at equilibrium. Validation of this method is carried out by examining the evolution of

adiabatic temperature T_f as a function the equivalence ratio ϕ, with the calculation results in [35], as shown in figure 10. A perfect match is seen, indicating that this method can be used to calculate the mass fractions of the species.

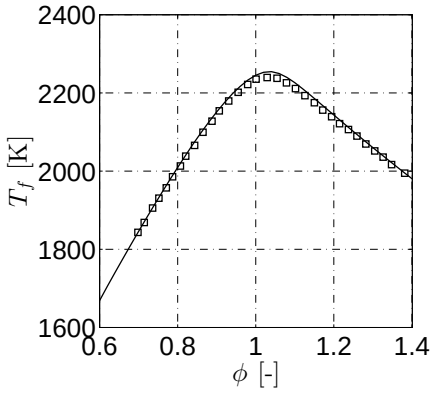

Figure 10: Evolutions of adiabatic temperature of methane-air flame as a function of the equivalence ratio ϕ. Markers: calculating results from [35]; solid line: current calculating results.

Acknowledgement

The authors would like to gratefully acknowledge the European Research Council (ERC) Starting Grant ACOULOMODE (2013-2018) for supporting the current research.

References

[1] J.R. Mahan and A. Karchemer. *Aeroacoustics of Flight Vehicles: Theory and Practice. Volume 1: Noise Sources*, volume 1, chapter Combustion and core noise, pages 483–517. WRDC Technical Report 90-3052, 1991.

[2] S. Candel. Combustion dynamics and control: Progress and challenges. *Proceedings of the Combustion Institute*, 29(1):1–28, 2002.

[3] S. Ducruix, T. Schuller, D. Durox, and S. Candel. Combustion dynamics and instabilities: Elementary coupling and driving mechanisms. *Journal of Propulsion and Power*, 19(5):722–734, 2003.

[4] S.M. Correa. Power generation and aeropropulsion gas turbines: From combustion science to combustion technology. *Proceedings of the Combustion Institute*, 27(2):1793–1807, 1998.

[5] T.C. Lieuwen and V. Yang, editors. *Combustion instabilities in gas turbines, Operational experience, Fundamental mechanisms, and Modeling*, volume 210 of *Progress in Astronautics and Aeronautics*. AIAA, Inc., 2005.

[6] A.P. Dowling and S.R. Stow. Acoustic analysis of gas turbine combustors. *Journal of Propulsion and Power*, 19(5):751–764, 2003.

[7] C.S. Goh and A.S. Morgans. The influence of entropy waves on the thermoacoustic stability of a model combustor. *Combustion Science and Technology*, 185(2):249–268, 2013.

[8] A.A. Peracchio and W.M. Proscia. Nonlinear heat-release/acoustic model for thermoacoustic instability in lean premixed combustors. *Journal of Engineering for Gas Turbines and Power*, 131(3):415–421, 1999.

[9] L. Crocco. Aspects of Combustion Stability in Liquid Propellant Rocket Motors Part I: Fundamentals. Low Frequency Instability With Monopropellants. *Journal of the American Rocket Society*, 21(6):163–178, 1951.

[10] M. Fleifil, A.M. Annaswamy, Z.A. Ghoneim, and A.F. Ghoniem. Response of a laminar premixed flame to flow oscillations: A kinematic model and thermoacoustic instability results. *Combustion and Flame*, 106(4):487–510, 1996.

[11] A.P. Dowling. Nonlinear self-excited oscillations of a ducted flame. *Journal of Fluid Mechanics*, 346:271–290, 1997.

[12] B.D. Bellows, Q. Zhang, Y. Neumeier, T. Lieuwen, and B.T. Zinn. Forced response studies of a premixed flame to flow disturbances in a gas turbine combustor. In *41st AIAA Aerospace Sciences Meeting and Exhibit*, number AIAA-2003-824, Reno, Nevada, USA, 2003.

[13] R. Balachandran, B.O. Ayoola, C.F. Kaminski, A.P. Dowling, and E. Mastorakos. Experimental investigation of the nonlinear response of turbulent premixed flames to imposed inlet velocity oscillations. *Combustion and Flame*, 143(1-2):37–55, 2005.

[14] D. Durox, T. Schuller, N. Noiray, and S. Candel. Experimental analysis of nonlinear flame transfer functions for different flame geometries. *Proceedings of the Combustion Institute*, 32(1):1391–1398, 2009.

[15] N. Karimi, M.J. Brear, S.H. Jin, and J.P. Monty. Linear and non-linear forced response of a conical, ducted, laminar premixed flame. *Combustion and Flame*, 156(11):2201–2212, 2009.

[16] D. Durox, J.P. Moeck, J.F. Bourgouin, P. Morenton, M. Viallon, T. Schuller, and S. Candel. Flame dynamics of a variable swirl number system and instability control. *Combustion and Flame*, 160(9):1729–1742, 2013.

[17] Lord Rayleigh. *Theory of Sound (two volumes)*. Dover Publications, New York, 1877, re-issued 1945.

[18] A.P. Dowling and A.S. Morgans. Feedback control of combustion oscillations. *Annual Review of Fluid Mechanics*, 37:151–182, 2005.

[19] T. Poinsot, D. Veynante, F. Bourienne, S. Candel, E. Esposito, and J. Surget. Initiation and suppression of combustion instabilities by active control. *Proceedings of the Combustion Institute*, 22(1):1363–1370, 1989.

[20] N. Noiray, D. Durox, T. Schuller, and S. Candel. A unified framework for nonlinear combustion instability analysis based on the flame describing function. *Journal of Fluid Mechanics*, 615:139–167, 2008.

[21] S. Schimek, J.P. Moeck, and C.O. Paschereit. An experimental investigation of the nonlinear response of an atmospheric swirl-stabilized premixed flame. *Journal of Engineering for Gas Turbines and Power*, 133(10):101502 (7 pages), 2011.

[22] F. Boudy, D. Durox, T. Schuller, G. Jomaas, and S. Candel. Describing function analysis of limit cycles in a multiple flame combustor. *Journal of Engineering for Gas Turbines and Power*, 133(6):061502 (8 pages), 2011.

[23] N. Noiray, M. Bothien, and B. Schuermans. Investigation of azimuthal staging concepts in annular gas turbines. *Combustion Theory and Modelling*, 15(5):585–606, 2011.

[24] J. Li and A.S. Morgans. Model based control of nonlinear combustion instabilities. In *the 21st International Congress on Sound and Vibration (ICSV21)*, Beijing, China, 2014.

[25] V. Bellucci, B. Schuermans, D. Nowak, P. Flohr, and C.O. Paschereit. Thermoacoustic modeling of a gas turbine combustor equipped with acoustic dampers. *Journal of Turbomachinery*, 127(2):372–379, 2005.

[26] A.S. Morgans and S.R. Stow. Model-based control of combustion instabilities in annular combustors. *Combustion and Flame*, 150(4):380 – 399, 2007.

[27] S.R. Stow and A.P. Dowling. A time-domain network model for nonlinear thermoacoustic oscillations. *Journal of Engineering for Gas Turbines and Power*, 131(3):031502 (10 pages), 2009.

[28] F.E. Marble and S.M. Candel. Acoustic disturbance from gas non-uniformities convected through a nozzle. *Journal of Sound and Vibration*, 55(2):225–243, 1977.

[29] A.S. Morgans and A.M. Annaswamy. Adaptive control of combustion instabilities for combustion systems with right-half plane zeros. *Combustion Science and Technology*, 180(9):1549–1571, 2008.

[30] T. Sattelmayer. Influence of the combustor aerodynamics on combustion instabilities from equivalence ratio fluctuations. *J. Eng. Gas Turbines Power*, 125(1):11–19, 2003.

[31] Aimee S. Morgans, Chee Su Goh, and Jeremy A. Dahan. The dissipation and shear dispersion of entropy waves in combustor thermoacoustics. *Journal of Fluid Mechanics*, 733(R2), 2013.

[32] S. Stow, A.P. Dowling, and T.P.Hynes. Reflection of circumferential modes in a choked nozzle. *Journal of Fluid Mechanics*, 467:215–239, 2002.

[33] P. Palies, D. Durox, T. Schuller, and S. Candel. Nonlinear combustion instability analysis based on the flame describing function applied to turbulent premixed swirling flames. *Combustion and Flame*, 158(10):1980–1991, 2011.

[34] Kenneth Kuan-yun Kuo. *Principles of Combustion*. Wiley-Interscience, New Jersey, 2005.

[35] C.K. Law, A. Makino, and T.F. Lu. On the off-stoichiometric peaking of adiabatic flame temperature. *Combust. Flame*, 145(4):808 – 819, 2006.